Improved Manifold Coordinate Representations of Hyperspectral Imagery

†Charles M. Bachmann ‡ Thomas L. Ainsworth † Robert A. Fusina
Naval Research Laboratory
Remote Sensing Division, †Code 7232, ‡ Code 7263
Washington, D. C. 20375
e-mail: bachmann@nrl.navy.mil

Abstract— **There are many well-known sources of nonlinearity present in hyperspectral imagery; these include bi-directional reflectance distribution function (BRDF) effects, multi-path scatter between heterogeneous pixel constituents, and the variable presence of water, an attenuating medium, in the scene. In recent publications, we have presented a data-driven approach to representing the nonlinear structure of hyperspectral imagery [4]. The approach relies on graph methods to derive geodesic distances on the high-dimensional hyperspectral data manifold. From these distances, a set of manifold coordinates that parameterizes the data manifold is derived. Because of the computational and memory overhead required in the geodesic coordinate calculations, the approach relies on partitioning the scene into subsets where the optimal manifold coordinates can be derived in an efficient manner, followed by an alignment stage during which the embedded manifold coordinates for each subset are aligned to a common manifold coordinate system. In [4], we demonstrated the feasibility of the coordinate and alignment methodology and the ability of the manifold approach to provide higher data compression and more effective classification when compared with linear methods. In this paper we develop an improved approach to the manifold coordinate alignment phase with an improved sampling methodology. Results are demonstrated using examples of hyperspectral imagery derived from PROBE2 hyperspectral scenes of the Virginia Coast Reserve barrier islands.**

I. Introduction and Background

A. Nonlinearity in Hyperspectral Imagery

Nonlinearity in hyperspectral imagery is a significant source of estimation errors in derived products. Sources of nonlinearity include: (1) nonlinear variations in reflectance produced by variations in sun-canopy-sensor geometry in the landscape [15] [9], (2) multi-path scatter among sub-pixel constituents [12] [14], violating the traditional linear mixing assumptions, (3) the variable presence of water, an attenuating medium [11] in the scene. Some of the errors that we observed in mapping products that we previously derived in [2] [3] became the motivation for finding new methods of modeling nonlinear structure in hyperspectral data [4]. In the next two subsections, we give a brief overview of the approach that we presented in [4] as a preamble to introducing improvements.

CMB and RAF were supported by the Office of Naval Research. CMB and RAF also acknowledge computing resources provided by the DOD High Performance Computing (HPC) Modernization Program, including the Maui High Performance Computing Center (MHPCC), the Army Research Laboratory's Major Shared Resource Center (ARLMSRC), and SMDC .

B. Manifold Coordinate Representations

In [4], we described a new method for modeling nonlinear effects in hyperspectral imagery and demonstrated that it provided a better means of discriminating land-cover types with a high-degree of spectral similarity. Using examples from AVIRIS and PROBE2 imagery, we also showed that our new approach provides better compression of HSI data in both terrestrial and aquatic imagery. The new method involves a data-driven estimation of a set of coordinates that parameterizes the high-dimensional hyperspectral data manifold. The method proceeds by calculating the local spectral neighborhood distances where linearity is assumed to hold about each sample and then determining the shortest nonlinear path (geodesic) distances to all other spectral samples outside the spectral neighborhood. These distances are then used to derive the manifold coordinate system that parameterizes the high-dimensional hyperspectral data manifold. In [4], we also described methods for achieving computationally scalable implementations of this approach. In Figure 1, we provide a conceptual representation of manifold coordinate estimation; note that the manifold coordinate system parameterizes the high-dimensional (124 channels in this example) HSI data manifold, so that linear distance in the coordinates corresponds to a nonlinear distance over the surface of the original higher-dimensional data. In Section IV, examples of this processing applied to PROBE2 hyperspectral imagery from our Virginia Coast Reserve barrier islands study site are provided.

The fundamental computational steps are: partition the scene into a set of computationally tractable "tiles", then the computation of a low-dimensional set of manifold coordinates using the Isometric Mapping (ISOMAP) [18] algorithm, and finally a manifold alignment stage using a reconstruction algorithm in which coordinate transformations are derived between the manifold coordinates of the tiles [4]. Note that the definition of "tractable" was addressed in [4], but improved scaling presented in Section II expands the scale of what is considered a computationally feasible tile size. The ISOMAP portion of the computations involves the following steps: (1) given a specified metric such as Euclidean, spectral angle, or some other appropriate choice, determine the spectral neighborhoods (initial sparse neighborhood graph) where linearity holds, maintaining a list for each sample of its neighbors and metric distances; (2) at each sample, for all distances outside the neighborhood, use

Report Documentation Page

Form Approved
OMB No. 0704-0188

1. REPORT DATE	2. REPORT TYPE	3. DATES COVERED
25 JUL 2005	**N/A**	**-**

4. TITLE AND SUBTITLE	
Improved Manifold Coordinate Representations of Hyperspectral Imagery	5a. CONTRACT NUMBER
	5b. GRANT NUMBER
	5c. PROGRAM ELEMENT NUMBER
6. AUTHOR(S)	5d. PROJECT NUMBER
	5e. TASK NUMBER
	5f. WORK UNIT NUMBER
7. PERFORMING ORGANIZATION NAME(S) AND ADDRESS(ES) **Naval Research Laboratory Remote Sensing Division, Code 7232, Code 7263 Washington, D. C. 20375**	8. PERFORMING ORGANIZATION REPORT NUMBER
9. SPONSORING/MONITORING AGENCY NAME(S) AND ADDRESS(ES)	10. SPONSOR/MONITOR’S ACRONYM(S)
	11. SPONSOR/MONITOR’S REPORT NUMBER(S)

12. DISTRIBUTION/AVAILABILITY STATEMENT
Approved for public release, distribution unlimited

13. SUPPLEMENTARY NOTES
See also ADM001850, 2005 IEEE International Geoscience and Remote Sensing Symposium Proceedings (25th) (IGARSS 2005) Held in Seoul, Korea on 25-29 July 2005. , The original document contains color images.

14. ABSTRACT

15. SUBJECT TERMS

16. SECURITY CLASSIFICATION OF:			17. LIMITATION OF ABSTRACT	18. NUMBER OF PAGES	19a. NAME OF RESPONSIBLE PERSON
a. REPORT	b. ABSTRACT	c. THIS PAGE			
unclassified	**unclassified**	**unclassified**	**UU**	**4**	

Standard Form 298 (Rev. 8-98)
Prescribed by ANSI Std Z39-18

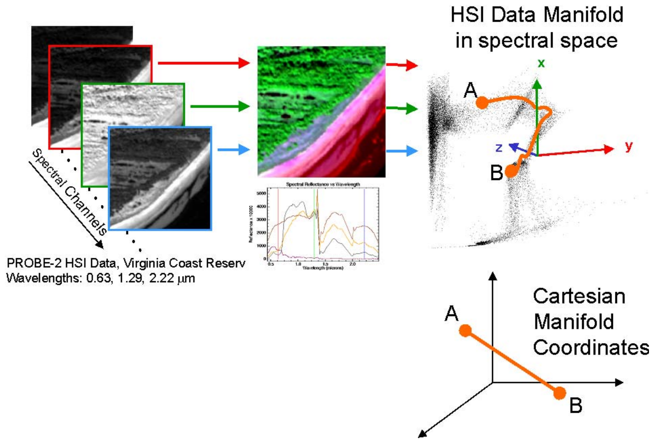

Fig. 1. Conceptual view of manifold coordinate system. (Left) PROBE2 image subset, showing the source data of 124 spectral channels. (Center) RGB triplet shows a false color image of the scene derived from wavelengths at 0.63, 1.29, and 2.22 μm for the subset over Smith Island, VA, October 18, 2001; shown: uplands, brackish and fresh water marshes, dunes, beach, and surf zone. (Right, top) Corresponding scatterplot of the reflectance of these arbitrarily chosen channels, reveal a highly nonlinear HSI data manifold. (Right, bottom) Manifold coordinate system parameterizes the HSI spectral data (note that the coordinates are a parameterization of the full spectral data, not just the three arbitrarily displayed channels).

Dijkstra's algorithm [7] [16] with a minimum priority queue to relax the closest edge not already attached to the graph d_G to compute the shortest nonlinear path (geodesic) distance to all other samples (note that this is a graph calculation and that the metric, therefore, is not involved here but is only evaluated in step (1) inside the neighborhood); (3) if there are any remaining distances which can not be connected in the distance graph, attach pockets of isolated points to each other in the graph by find the closest linear distance between pairs of isolated pockets, thus preserving the geodesic structure of each and ensuring a minimal spanning tree [4] [1]; after attaching all points symmetrize to ensure consistency of paths in both directions; (4) with the full NxN (N=number of spectral samples) geodesic distance matrix calculated in steps (1) and (2), compute the second order variation in the geodesic distances, $\tau = -\frac{1}{2}H^T SH$, where $S_{ij} = ((d_G)_{ij})^2$ and $H_{ij} = \delta_{ij} - \frac{1}{N}$ is a centering matrix ; and (5) extract s ($s << N$) manifold coordinates from the most significant eigenvectors and eigenvalues of the NxN matrix τ with the ith manifold coordinate given by $\vec{M}_i = \sqrt{\lambda_i}\vec{v}_i$.

C. Scalable Algorithms

In [4], we addressed the computational and memory scaling issues associated with manifold coordinate calculations at remote sensing scales where we may typically want to process $O(10^6 - 10^7)$ pixels in a single hyperspectral scene. One of the principal limiting factors was memory which scaled as $O(N^2)$ because of the need to store d_G. Computationally, the Dijkstra alogrithm with a minimum priority queue implementation [16] ensures that the graph calculation scales as $O(N^2 log(N))$. Because of the computational and memory requirements, we developed a scaling strategy [4] in which large hyperspectral scenes are divided into a computationally tractable set of data blocks or "tiles" for which manifold coordinates can be optimally computed, followed by an alignment phase during which the embedded manifold coordinates for each tile subset are aligned to a common manifold coordinate system.

In [4], several strategies for alignment were proposed. These included: (a) splicing a set of common samples onto each tile which could serve as guide-posts for manifold alignment, (b) partitioning the scene into tiles by random or active sampling followed by an alignment stage, and finally (c) a direct reconstruction technique, in which full spectral samples from one tile (derived from the original scene or a decimated subset) were reconstructed in the spectral space of another tile using the locally linear property of the manifold. The same set of transformations apply equally in the manifold coordinate and the full spectral space. By reconstructing enough samples where there is sufficient data in each tile for accurate reconstruction, a coordinate transformation can be derived using the pseudoinverse:

$$P = (M_i^T M_i)^{-1} M_i^T M_j^* \quad (1)$$

where M_i is the matrix of manifold coordinate samples from tile T_i and M_j^* is the corresponding set of coordinates reconstructed in the manifold coordinate system of tile T_j. When no sufficiently accurate reconstruction was possible to a prechosen target tile, a series of alignment hops was used between intermediate tiles possessing common features of source and target tiles.

The reconstruction method was determined to be the most effective of the manifold alignment strategies, with the others less effective, primarily because of sampling limitations that result from restrictions on tile size imposed by memory limitations. In the next section, however, we incorporate a method which allows the d_G to be replaced by a significantly smaller but representative matrix that mitigates the memory burden. The reduced memory requirements of the modified approach allow for several of these alignment strategies to be used more practically or in combination, although because of limited space we only demonstrate the advantages of the improved scaling for the manifold alignment strategy based on the reconstruction principle of Equation 1. In addition, to lower memory requirements, the method described in the next Section also streamlines other computational issues such as the eigensolution of τ, eliminating iterative eigensolvers in favor of more reliable exact solvers appropriate to smaller matrices, and also results in fewer geodesic distances calculations (the $O(N^2 log(N)$ Dijkstra calculation is now replaced with an $O(LNlog(N))$ calculation with $L << N$.

With the new method described in the next Section, another additional benefit is that the probability of alignment errors should be lower since the size of each tile can be larger and more representative of the scene. This will help to eliminate occasional alignment errors that appeared originally in [4] which resulted from incomplete constraint of manifold coordinates between tiles, stemming from the limited sampling available in each tile. However, one potential challenge with larger tiles is

[1] Note that this can be accomplished by iteratively attaching the closest unattached sample to the graph and then running the Dijkstra algorithm on the first row of d_G until all points have a path to the first point; this ensures efficient scaling of $O(\alpha N log(N))$ with $\alpha << N$ in most cases

that more constraints must be satisfied in each alignment because of the greater diversity of spectral samples represented in each tile; this potentially requires a more flexible local reconstruction error criterion that potentially takes account of other issues such as sample density. A full discussion of the latter will be taken up in future publications.

II. Improved Scaling for Manifold Coordinate Representations

An improvement to the processing speed and memory requirements associated with ISOMAP was described in [6]. The improved method chooses a set of "landmarks" (L-ISOMAP) from which all of the manifold geodesic distances d_G are calculated. This forms an LxN geodesic distance matrix with $L << N$. The symmetric submatrix d_L of distances between landmarks is an LxL matrix whose eigenvalues and eigenvectors form the basis of the embedding of the manifold coordinates. Note that so long as the sampled landmarks span the space of the embedded manifold coordinates, the landmark distances are sufficient to calculate the manifold coordinate system. Note also that the eigenvector and eigenvalue problem of a large NxN matrix has been replaced by a smaller LxL problem. As before, the second order variation in d_L is computed according to: $\tau_L = - - \frac{1}{2} H^T S_L H$, where $(S_L)_{ij} = ((d_L)_{ij})^2$. For τ, iterative methods [17] were used to extract the eigenspectrum, however, with the LxL matrix τ_L, more reliable exact eigensolvers can be employed. Once the most significant eigenvalues and eigenvectors of τ_L have been determined, the manifold coordinates of the remaining non-landmark samples can be computed by a simple linear transformation since their distances to the landmark positions are all known:

$$M(\vec{x}) = P_L * ((\bar{\Delta} - \Delta) \tag{2}$$

where $M(\vec{x})$ is the embedded manifold coordinate of spectral sample x, P is a matrix whose ith row is:

$$(P_L)_i = \frac{(\vec{v}_L)_i}{\sqrt{(\lambda_L)_i}} \tag{3}$$

where $(\vec{v}_L)_i$ and $(\lambda_L)_i$ are the ith eigenvector and eigenvector of τ_L, $\bar{\Delta}_i = E_{L_j}(((d_L)_{L_i L_j})^2)$ is the mean squared distance from the ith landmark to all other landmarks, and $\Delta_{ij} = ((d_L)_{L_i j})^2$ is the squared distance from sample j to the ith landmark.

III. Hyperspectral Time Series and Study Site

In May 2000, we began airborne hyperspectral data acquisitions over a subset of the Virginia barrier islands, collectively known as the Virginia Coast Reserve [19] [10] [13] show in Figure 2. A time series of airborne hyperspectral images has been collected over the region outlined in boxes in Figure 2. Beginning with a single scene over Smith Island, VA in May 2000 by HyMAP, acquisitions have continued to the present day and have included scenes covering the seven islands between Smith and Hog Islands inclusive in summer and fall of 2001 and 2002. Parramore Island was also added during the 2002 fall collection and included in all subsequent collections. COMPASS acquired data over the same set of islands in fall 2003. In 2004, the Naval Research Laboratory's PHILLS [8] began acquiring imagery over the island chain twice annually in spring and summer.

Fig. 2. Virginia Coast Reserve study area and adjacent mainland (Northampton and Accomack counties) shown in a Landsat TM image from August 6, 1999. Red boxes outline regions where our airborne hyperpspectral imagery time series has been collected between 2000-2005 by a variety of sensors including HyMAP, PROBE2, COMPASS, and PHILLS.

One focus of our research at the Virginia Coast Reserve site has been the devlopment and testing of algorithms for detailed species-level mapping of coastal land-cover [2] [3] [1] [4]. Using the hyperspectral time series, we have developed fast online methods for fusing the clasification results from multi-temporal inputs, for example, mapping products developed for different seasons [3]. The fusion of classifier results uses smooth estimated measures of classifier reliability to determine a final category at each pixel. Extensive ground truth data has been collected by us [2] [3] throughout all of the islands in the chain, including both *in situ* reflectance data, BRDF, and more recently biophysical data including biomass, canopy light penetration, leaf area index (LAI), and leaf optical measurements [5].

IV. Results

Our first example illustrates the advantage of L-ISOMAP applied to the problem of single tile optimization. Because computational and memory requirements are lower for L-ISOMAP, we are able to derive the manifold coordinates directly for whole cross-sections of the scene treated as a single tile; typically this means an increase in tile size by more than an order of magnitude when compared with the tile size used in [4] (see Figure 3). In Figure 4, we show an example derived from one of these enlarged tiles taken from the northern end of the Smith Island PROBE2 hyperspectral scene originally depicted in Figure 4. Also shown are example manifold coordinates (2-3-4) derived using the L-ISOMAP processing. This end of Smith Island is dominated by salt marsh, dunes, beach, and tidal estuaries and channels connecting to the Atlantic Ocean. A rich structure related to species distribution and perhaps biophysical parameters is delineated in the manifold coordinates. In our

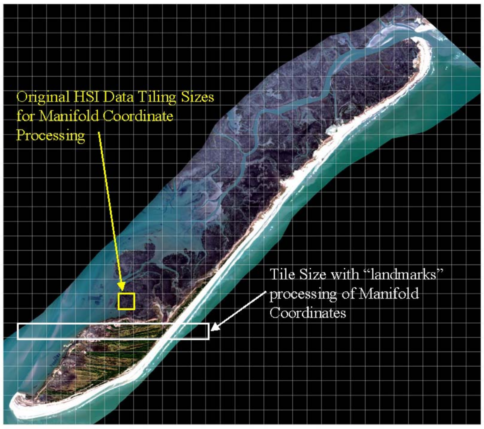

Fig. 3. RGB image derived from PROBE2 HSI scene of Smith Island, VA acquired October 18, 2001, and typical tile size used in our previously published alignment of tile HSI manifold coordinates, showing an N=(75x75) pixel tile size. Note that because second order geodesic distance matrix τ is O(N^2) a machine memory limit of 1GB would impose a tile size limit of N=(105x105). Also shown, typical tile size made possible by landmarks processing which has memory requirements of O(LN) with $L << N$.

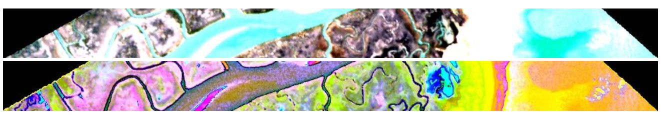

Fig. 4. (Top) Subset of PROBE2 hyperspectral scene shown in Figure 3: a cross-section of the northern end of Smith Island. (displayed wavelengths: 0.65, 0.55, 0.45 μm). (Bottom) Manifold coordinates 2-3-4 obtained using L-ISOMAP, showing extensive structure in marsh zones and shallow water.

second example (Figure 5), we portray the alignment of two of these enlarged tiles for another scene of Hog Island, VA taken by PROBE2, also on October 18, 2001. The Figure shows a section of the northern end of Hog Island, with a diverse cross-section of the island portrayed, including salt marsh, upland zones, brackish and fresh water marsh species, dune environment, and beaches. This island subset was partitioned into two different cross-island swaths (tiles); manifold coordinates were obtained using L-ISOMAP and then the manifold coordinates were aligned using the method described in [4].

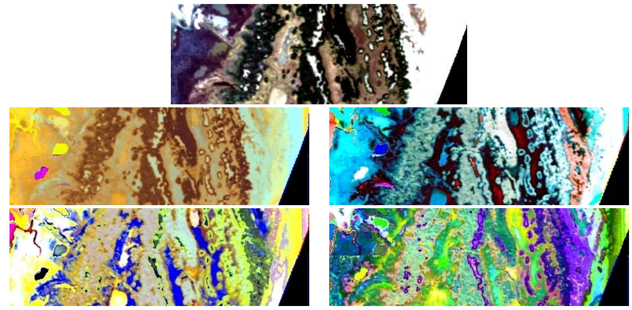

Fig. 5. Manifold coordinates for a subset of (top) a PROBE2 hyperspectral scene of Hog Island, VA on October 18, 2001, revealing details about species-level spatial distributions. Coordinate combinations shown are (middle, left) 1-2-3, (middle, right) 4-5-6, (bottom, left) 7-8-9, (bottom,right) 10-11-12. Using L-ISOMAP the manifold coordinates were optimized for the two tiles comprising the subset. The tiles were cross-sectional rows of size 75x825 and 75x750 pixels (only the land subset of these tiles is shown here). The manifold coordinates were aligned using the method described in [4].

REFERENCES

[1] C. M. Bachmann, "Improving the Performance of Classifiers in High-Dimensional Remote Sensing Applications: An Adaptive Resampling Strategy for Error-Prone Exemplars (ARESEPE)," *IEEE Trans. on Geosci. Remote Sensing*, vol. 41, no. 9, pp 2101-2112, 2003.

[2] C. M. Bachmann, T. F. Donato, G. M. Lamela, W. J. Rhea, M. H. Bettenhausen, R. A. Fusina, K. DuBois, J. H. Porter and B. R. Truitt, "Automatic Classification of Land-Cover on Smith Island, VA Using HYMAP Imagery," *IEEE Trans. Geosci. Remote Sensing,* Vol. 40, No. 10, pp. 2313-2330, 2002.

[3] C. M. Bachmann, M. H. Bettenhausen, R. A. Fusina, T. F. Donato, A. L. Russ, J. Burke, G. M. Lamela, W. Joseph Rhea, B. R. Truitt, J. H. Porter, "A Credit Assignment Approach to Fusing Classifiers of Multi-Season Hyperspectral Imagery," *IEEE Trans. Geosci. Remote Sensing,* vol. 41, no. 11, pp. 2488-2499, 2003.

[4] C. M. Bachmann, T. L. Ainsworth, R. A. Fusina, "Exploiting Manifold Geometry in Hyperspectral Imagery," *IEEE Transactions on Geoscience and Remote Sensing,* Vol. 43, No. 3, pp. 441-454, 2005.

[5] C. M. Bachmann, T. L. Ainsworth, R. A. Fusina, T. F. Donato, J. Bowles, D. Korwan, E. Ramsey III, A. Rangoonwala, G. Nelson, J. Sellars, "Using Hyperspectral Imagery to Link Land-Cover Models and Biophysical Parameter Estimates: a Case Study in the Virginia Coast Reserve," Proc. Eighth International on Remote Sensing for Marine and Coastal Environments, Halifax, Nova Scotia, May 17-19, 2005.

[6] V. de Silva, J. B. Tenenbaum, "Global versus local methods in nonlinear dimensionality reduction," in Advances in Neural Information Processing Systems 15. S. Becker, S., Thrun, S., and Obermayer, K. (eds). Cambridge, MIT Press, pp. 705-712, 2002.

[7] E. W. Dijkstra, "A note on two problems in connexion with graphs. *Numerische Mathematik*, Vol. 1, pp. 269-271, 1959.

[8] C. O. Davis, J. Bowles, R. A. Leathers, D. Korwan, T. V. Downes, W. A. Snyder, W. J. Rhea, W. Chen, J. Fisher, W. P. Bissett, R. A. Reisse, "Ocean PHILLS hyperspectral imager: design, characterization, and calibration," Optics Express, Vol. 10, No. 4, pp. 210-221, 2002.

[9] D. G. Goodin, J. Gao, G. M. Henebry, "The Effect of Solar Illumination Angle and Sensor View Angle on Observed Patterns of Spatial Structure in Tallgrass Prairie, " *IEEE Trans. Geosci. and Remote Sensing*, vol. 42, no. 1, pp. 154-165.

[10] Web site for the University of Virginia's Long Term Ecological Research Program. [Online]. Available: http://www.vcrlter.virginia.edu

[11] C. D. Mobley, *Light and Water: Radiative Transfer in Natural Waters*, Academic Press, San Diego, 1994.

[12] J. F. Mustard, L. Li, G. He, "Nonlinear spectral mixture modeling of lunar multispectral data: Implications for lateral transport," *Journal of Geophysical Research,* Vol. 103, No. E8, pp. 19419-19425, August 25, 1998.

[13] Web site for NASA EOS Land Validation Core Site [Online]. Available: http://landval.gsfc.nasa.gov/MODIS/coresite.php?SiteID=27

[14] D. A. Roberts, M. O. Smith, J. B. Adams, "Green Vegetation, nonphotosynthetic vegetation, and soils in AVIRIS data," *Remote Sensing of Environment*, Vol. 44, pp. 255-269, 1993.

[15] S. R. Sandmeier, E. M. Middleton, D. W. Deering, W. Qin, "The potential of hyperspectral bidirectional reflectance distribution funciton data for grass canopy characterization," *Journal of Geophysical Research*, Vol. 104, No. D8, pp. 9547-9560, April 27, 1999.

[16] R. Sedgewick, *Algorithms in C++, Part 5: Graph Algorithms*, Addison-Wesley, Boston, 2002.

[17] G. Sleijpen, H. van der Vorst, "Jacobi-Davidson Methods", available online, http://www.cs.utk.edu/ dongarra/etemplates/node136.html through http://www.cs.utk.edu/ dongarra/etemplates/note147.html, 1994.

[18] J. B. Tenenbaum, V. de Silva, J. C. Langford, "A Global Geometric Framework for Nonlinear Dimensionality Reduction," *Science*, Vol. 290, pp. 2319-2323, December 22, 2000.

[19] Web site for The Nature Conservancy's Virginia Coast Reserve [Online]. Available: http://nature.org/wherewework/northamerica/states/virginia/preserves/art1244.html.